Transport behavior of coupled continuous-time random walks

Marco Dentz
Department of Geotechnical Engineering and Geosciences, Technical University of Catalonia (UPC), Barcelona, Spain

Harvey Scher, Devora Holder, and Brian Berkowitz
Department of Environmental Sciences and Energy Research, Weizmann Institute of Science, 76100 Rehovot, Israel

(Received 16 May 2008; published 8 October 2008)

The origin of anomalous or non-Fickian transport in disordered media is the broad spectrum of transition rates intrinsic to these systems. A system that contains within it heterogeneities over multiple length scales is geological formations. The continuous time random walk (CTRW) framework, which has been demonstrated to be an effective means to model non-Fickian transport features in these systems and to have predictive capacities, has at its core this full spectrum represented as a joint probability density $\psi(\mathbf{s},t)$ of random space time displacements $(\mathbf{s},t)$. Transport in a random fracture network (RFN) has been calculated with a coupled $\psi(\mathbf{s},t)$ and has subsequently been shown to be approximated well by a decoupled form $\psi(\mathbf{s},t)=F(\mathbf{s})\psi(t)$. The latter form has been used extensively to model non-Fickian transport in conjunction with a velocity distribution $\Phi(\xi),\xi\equiv 1/v$, where v is the velocity magnitude. The power-law behavior of $\psi(t)\propto t^{-1-\beta}$, which determines non-Fickian transport, derives from the large ξ dependence of $\Phi(\xi)$. In this study we use numerical CTRW simulations to explore the expanded transport phenomena derived from a coupled $\psi(\mathbf{s},t)$. Specifically, we introduce the features of a power-law dependence in the $\mathbf{s}$ distribution with different $\Phi(\xi)$ distributions (including a constant v) coupled by $t=s\xi$. Unlike Lévy flights in this coupled scenario the spatial moments of the plumes are well defined. The shapes of the plumes depend on the entire $\Phi(\xi)$ distribution, i.e., both small and large ξ dependence; there is a competition between long displacements (which depend on the small ξ dependence) and large time events (which depend on a power law for large ξ). These features give rise to an enhanced range of transport behavior with a broader scope of applications, e.g., to correlated migrations in a RFN and in heterogeneous permeability fields. The approximation to the decoupled case is investigated as a function of the nature of the $\mathbf{s}$ distribution.

DOI: 10.1103/PhysRevE.78.041110 PACS number(s): 05.40.Fb, 05.60.−k, 02.50.−r, 05.10.Gg

I. INTRODUCTION

The theory of transport in disordered systems has been an active subfield of a number of areas of science and engineering for decades [1]. The applications cover an enormous range of length and time scales. A system that contains within it intrinsic heterogeneities over multiple length scales is geological formations [2–4]. Chemical plumes migrating in the complex saturated flow fields of these formations have been observed to exhibit highly anomalous or non-Fickian forms. Recent theoretical approaches have emphasized that the cause of the latter behavior is due to the broad spectrum of rates or transition times engendered by these heterogeneities [5]. In this spectrum, statistically rare events, such as an encounter with a low velocity transition, have an especially large effect on the dispersion of the migrating plume. This fundamental feature of the disordered system clearly demonstrates the need to take into account the full spectrum of these transition times and not just the aggregate average rate at each length scale. We have used the approach of a continuous time random walk (CTRW) [5], which has at its core a spectrum represented as a joint probability density $\psi(\mathbf{s},t)$ of random space time displacements $(\mathbf{s},t)$. What is the origin of $\psi(\mathbf{s},t)$ and how does it relate to the spectrum of rates?

The nonlocal-in-time transport equation that embodies $\psi(\mathbf{s},t)$ has been shown to be the ensemble average of the master equation, which contains all of the aforementioned rates, denoted $w(\mathbf{s},\mathbf{s}')$ for a transition between $\mathbf{s}$ and $\mathbf{s}'$ [6]. The $\psi(\mathbf{s},t)$ is a functional of $w(\mathbf{s},\mathbf{s}')$ (Appendix B of Ref. [5]) and has been determined analytically [7] for sets of $w(\mathbf{s}-\mathbf{s}')$. Numerical simulations of a spectrum of local transits (derived from local displacements and velocities) have been used to obtain $\psi(\mathbf{s},t)$ on the field scale [8], the pore scale [9], two-dimensional random fracture networks (RFNs) [6] and idealized conductivity fields [10–12]. In the CTRW framework the entire plume can be calculated and has been characterized by a few features of $\psi(\mathbf{s},t)$ as shown in Fig. 1 [5]; namely, the power-law (dependence) region of the zeroth spatial moment of $\psi(\mathbf{s},t)$, $\psi(t)\sim t^{-1-\beta}$, where $0<\beta<2$ and the cutoff or transition region to $\beta>2$. Both regions are a

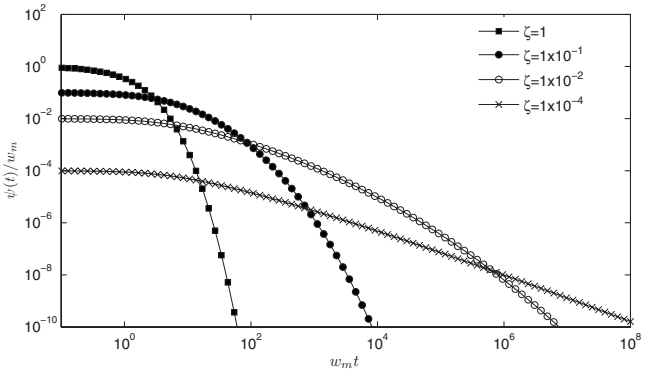

FIG. 1. Log-log plot of dimensionless $\psi(t)$ vs dimensionless time τ. The power-law $[\psi(t)\propto t^{-1-\beta}]$ region and the cutoff behavior $(\beta>2)$ region depend on the disorder parameter ζ; see text for definition of w_m and ζ.

function of the system disorder, which is determined by the parameter ζ (in the context of electron hopping in a random array of sites [Eqs. (22), (23), of Ref. [5]] with an electron transfer rate of $w_m \exp(-|\mathbf{s}-\mathbf{s}'|/r_0)$, and $\zeta=4\pi N_s r_0^3$, where N_s is the site density). The extent of the power-law region determines the observational duration of the anomalous or non-Fickian transport and the extent of the cutoff region determines the time span of the transition to normal transport.

The emphasis in this picture has been on the significant effect of statistically rare large time transitions, e.g., due to an encounter with a low velocity zone, i.e., a high inverse velocity ξ ($\xi \equiv 1/v, \xi \geqslant 0$, where $v=|\mathbf{v}|$ is the absolute particle velocity). This encounter is enhanced if the ξ dependence of the velocity distribution function $\Phi(\xi)$ is a power-law tail. However, another possibility for a significant statistically rare event is a large displacement (compared to the median displacement) if a system, e.g., a RFN, has a power-law $\mathbf{s}$ distribution. The contribution of such displacements to the plume transport at a given time would depend on a sampling of the higher velocities, i.e., the small ξ end of $\Phi(\xi)$. These types of events clearly demonstrate the need for a coupled $\psi(\mathbf{s},t)$ between a power law in time and a Lévy [13,14] walk in space [15–17]. An efficient and flexible technique for dealing with the coupling of various distributions of $\mathbf{s}$ and ξ is numerical simulation of CTRW [18]. In Sec. II we present the coupled CTRW, in Sec. III we develop the simulation technique, in Sec. IV we specify the spatial distribution and the $\Phi(\xi)$ that comprise the coupled $\psi(\mathbf{s},t)$, and in Sec. V follow with the details of our results and discussion.

II. COUPLED CONTINUOUS TIME RANDOM WALKS

Simply stated, in the CTRW a particle undergoes a random walk in space and time. The CTRW can be developed by analytical or numerical solution of a temporally nonlocal transport equation [5] and equivalently by numerical simulation [18] of the equation of motion of a particle in space-time. In the following we formulate a space-time coupled CTRW model and develop a Lagrangian formulation in terms of the spatiotemporal particle trajectories.

In this formulation of particle trajectories, if at each step the spatial and time increments are selected from independent distributions $F(\mathbf{s})$ and $\psi(t)$, respectively, the walk is denoted as the decoupled case. In the coupled case the distributions are not independent. There are many couplings and correlations that can be accommodated by the simulation methodology, defined below, due to its basic simplicity. There can be a direct mechanistic relation $t(s)$, e.g., $t^{\nu} \propto s$ [15] or through the introduction of the distribution of velocities (the case considered in this paper). The conditional distribution of (ξ,s) is $\Phi(\xi|s)$, or as we assume ξ independent of s, $\Phi(\xi|s)=\Phi(\xi)$. The basic coupling between the distributions occurs with the space-time link of $t=s\xi$. For the $\Phi(\xi)$ case especially there is no waiting time (or particle immobility). There are constant incremental transitions with random rates (i.e., velocities) between sites. Further examples can describe a nonstationary case both in space and/or time, e.g., $\Phi_{\mathbf{s}}(\xi)$, and correlation between successive steps, e.g., a choice of ξ depends on the choice at the previous step. This latter correlation has been studied in log permeability models [19]. These considerations as well as others are reserved for future studies.

Specifically, particle transport derived from fluid flow in disordered media can be characterized statistically by distributions of transition length, particle velocities and transition times. These distributions are in general coupled. We consider simulations that are determined by two given probability distributions functions (PDFs), one in $\mathbf{s}$ and the other in ξ; the angular direction of ξ, ω, is chosen to be that of $\mathbf{v}$, which is the direction of $\mathbf{s}$.

A. Spatial transitions

The angular dependence is associated with the velocity to best represent the effect of the bias (i.e., the pressure gradient across the flow domain), however, the ω dependence will be included in integrals over $\mathbf{s}$ [6]. The PDF for $\mathbf{s}$ is the marginal distribution

$$F(\mathbf{s}) = \int_0^{\infty} dt \psi(\mathbf{s},t), \tag{1}$$

which we specialize to

$$F(\mathbf{s})d\mathbf{s} = s^{d-1}p(s)ds\Omega(\omega)d\omega, \tag{2}$$

where the angle vector ω is distributed according to $\Omega(\omega)$. We work in spherical coordinates and we have simplified the ω dependence to a product form. A more elaborate version of treating angular dependence was used to model the velocity histogram of a RFN [6]. In this coordinate system it is understood that $s^{d-1}p(s)$ is the transition length distribution and we concentrate on forms for $p(s)$ below. The Cartesian coordinates x_i of the position vector $\mathbf{s}$ are given by

$$x_i = sf_i(\omega) \tag{3}$$

with $i=1,\ldots,d$, $f_i(\omega)$ the direction functions. For $d=2$ dimensions (2D), $f_1(\omega)=\cos(\omega)$ and $f_2(\omega)=\sin(\omega)$; for $d=3$, $\omega=(\omega,\theta)^T$ and $f_1(\omega)=\cos(\omega)\sin(\theta)$, $f_2(\omega)=\sin(\omega)\sin(\theta)$, and $f_3(\omega)=\cos(\theta)$.

We present expressions using the latter forms but all our simulation results here are performed in 2D domains. For the 2D case we use two normalized versions of $\Omega(\omega)$: a uniform distribution

$$\Omega_u(\omega) = \frac{2}{\pi}\Theta\left(\frac{\pi^2}{16} - \omega^2\right) \tag{4}$$

and a normal distribution

$$\Omega_n(\omega) = \exp(-\omega^2/2\sigma_n^2)/\sigma_n\sqrt{2\pi}, \tag{5}$$

where $\Theta(\chi)$ is the Heaviside function.

In this work we study the effects of different types of distributions of $p(s)$ and $\Phi(\xi)$. The distributions $F(\mathbf{s})$, $\Phi(\xi)$ are each normalized and

$$\psi(\mathbf{s},t) = F(\mathbf{s})\frac{\Phi(t/s)}{s}, \tag{6}$$

where we used the relation $\delta(s\xi - t) = \delta(\xi - \frac{t}{s})/s$. The spatial moments of $\psi(\mathbf{s},t)$ are

$$\mu_i^{(1)}(t) = a_i \mu^{(1)}(t), \quad \mu_{ij}^{(2)} = b_{ij}\mu^{(2)}(t), \tag{7}$$

where

$$\mu^{(\iota)}(t) = \int_0^\infty ds s^{d-2} s^\iota p(s)\Phi(t/s) \tag{8}$$

and

$$a_i = \int d\omega \Omega(\omega) f_i(\omega), \quad b_{ij} = \int d\omega \Omega(\omega) f_i(\omega) f_j(\omega). \tag{9}$$

For 2D and Eqs. (4) and (5), respectively, $a_i = \delta_{i,1}[2\sqrt{2}/\pi, \exp(-\sigma_n^2/2)]$ and $b_{ij} = \delta_{i,j} b_i, b_{3/2\mp 1/2} = [1/2 \pm 1/\pi, 1/2 \pm \exp(-2\sigma_n^2)/2]$, where $\delta_{i,j}$ is the Kronecker delta function. The marginal transition time distribution is given by [note that $\int d\omega \Omega(\omega) = 1$]

$$\psi(t) = \int ds s^{d-2} p(s)\Phi(t/s). \tag{10}$$

Frequently in the literature, decoupled CTRW models are used [5]. For these models the joint transition length and time distributions are independent according to

$$\psi_{\mathrm{dc}}(\mathbf{s},t) = F(\mathbf{s})\psi(t), \tag{11}$$

where the subscript dc denotes decoupled. The spatial moment factor (8) of Eq. (11) varies only with $F(\mathbf{s})$

$$\mu_{\mathrm{dc}}^{(\iota)}(t) = \psi(t)\int_0^\infty ds s^{d-1} s^\iota p(s). \tag{12}$$

In Ref. [5] the conditions are discussed whereby a coupled model can be approximated by Eq. (11). In the following we investigate this extensively and compare fully coupled models and their decoupled counterparts.

B. Space-time random walk

The defining distribution of the CTRW $\psi(\mathbf{s},t)$ forms the kernel of a nonlocal transport equation for the probability per time and space for a particle to just arrive at $(\mathbf{s},t)$ after $N+1$ steps, $R_{N+1}(\mathbf{s},t)$ [20]:

$$R_{N+1}(\mathbf{s},t) = \int_{\mathcal{L}^d} d^d s' \int_0^t dt' \psi(\mathbf{s}-\mathbf{s}', t-t') R_N(\mathbf{s}',t'), \tag{13}$$

where $\mathcal{L}^d$ denotes the d-dimensional transport domain. To derive an expression for the spatial distribution of particles, we define the probability per time and space for a particle to just arrive in $(\mathbf{s},t)$ by summation of $R_N(\mathbf{s},t)$ over all N:

$$R(\mathbf{s},t) \equiv \sum_{N=0}^{\infty} R_N(\mathbf{s},t). \tag{14}$$

Thus one obtains from Eq. (13) by summation over N [20]:

$$R(\mathbf{s},t) = \rho(\mathbf{s})\delta(t) + \int_{\mathcal{L}^d} d^d s' \int_0^t dt' \psi(\mathbf{s}-\mathbf{s}', t-t') R(\mathbf{s}',t'), \tag{15}$$

where we specified the initial condition $R_0(\mathbf{s},t) = \rho(\mathbf{s})\delta(t)$ of the CTRW.

The normalized resident concentration $c(\mathbf{s},t)$ is defined by the probability a solute particle can be found at $\mathbf{s}$ at time t. Thus, in terms of a CTRW, $c(\mathbf{s},t)$ is given by the sum over all probabilities that a solute particle reaches $\mathbf{s}$ at some time t' and the transition to the next site takes longer than $t-t'$ [20]:

$$c(\mathbf{s},t) = \int_0^t dt' \Psi(t-t') R(\mathbf{s},t'), \tag{16}$$

$$\Psi(t) = \int_t^\infty dt' \psi(t'). \tag{17}$$

In the following, we focus on vertically integrated particle distributions

$$\bar{c}(x_1,t) = \int d\mathbf{y} c(\mathbf{s},t), \tag{18}$$

where $\mathbf{y} = (x_2, \ldots, x_d)^T$. The pressure gradient over the domain is assumed to be in the one-direction. The first and second moments of $\bar{c}(x_1,t)$ give valuable information on the position of the center of mass of the particle distribution and its overall spread. They are defined by

$$m^{(1)}(t) = \int dx_1 x_1 \bar{c}(x_1,t), \tag{19a}$$

$$m^{(2)}(t) = \int dx_1 x_1^2 \bar{c}(x_1,t), \tag{19b}$$

respectively. The standard deviation measures the plume width and is defined by

$$\sigma(t) = [m^{(2)}(t) - m^{(1)}(t)^2]^{1/2}. \tag{20}$$

III. NUMERICAL RANDOM WALK SIMULATIONS

In principle, Eqs. (15) and (16) can be solved analytically or numerically for a given $\psi(\mathbf{s},t)$ and domain boundary conditions. One technical difficulty sometimes encountered is a numerical evaluation of the inverse Laplace transform. Another complementary approach is numerical simulation [18] via the application of the equations of motion given by the coupled Langevin equations

$$\mathbf{s}^{(N+1)} = \mathbf{s}^{(N)} + \boldsymbol{\varsigma}^{(N)}, \tag{21}$$

$$t^{(N+1)} = t^{(N)} + \tau^{(N)}, \tag{22}$$

where $(\mathbf{s}^{(N)}, t^{(N)})$ denotes the location of a particle in space-time after N steps. The spatial and temporal random increments $\boldsymbol{\varsigma}^{(N)}$ and $\tau^{(N)}$ are distributed according to the joint tran-

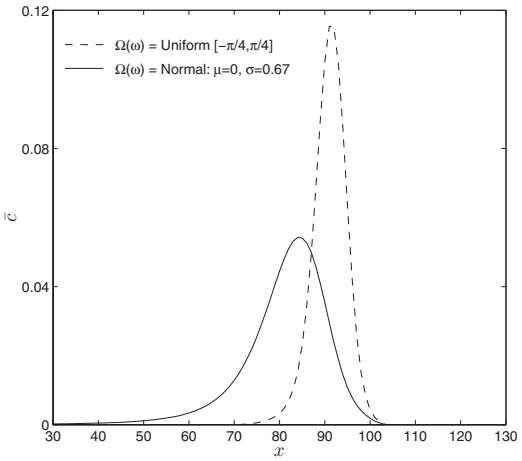

FIG. 2. Plot of the vertically integrated plume $\bar{c}(x,t)$ at $t=100$ resulting from a narrow $p(\mathbf{s})\sim$TPL ($\alpha=2.5$) and $\Phi(\xi)\sim\delta(\xi-\xi_0)$ ($\xi_0=1$), varying the form of $\Omega(\omega)$ as a uniform $[-\pi/4,\pi/4]$ and normal ($\sigma_n=0.67$, $\mu=0$) distribution.

sition displacement and time distribution $\psi(\mathbf{s},t)$. The analytical and simulation approaches were compared in Ref. [18] and the agreement is excellent. In the simulation method of solution for the particle distribution (21) and (22) after N steps, $R_N(\mathbf{s},t)$ (13) can be expressed in terms of the particle trajectories in space time [21]

$$R_N(\mathbf{s},t)=\langle\delta(\mathbf{s}-\mathbf{s}^{(N)})\delta(t-t^{(N)})\rangle, \tag{23}$$

where the angular brackets denote the average over all realizations of $\{\mathbf{s}^{(N)}\}$ and $\{\tau^{(N)}\}$. Expression (23) is the representation of $R_N(\mathbf{s},t)$ in the context of random walk simulations, which will be determined in this paper. Using definition (14) of $R(\mathbf{s},t)$ and the representation (23) of $R_N(\mathbf{s},t)$, we derive

$$c(\mathbf{s},t)=\sum_{N=0}^{\infty}\int_0^t dt'\Psi(t-t')\langle\delta(\mathbf{s}-\mathbf{s}^{(N)})\delta(t'-t^{(N)})\rangle. \tag{24}$$

Knowing the entire time history of the flux (aggregate trajectories) entering a small volume around $\mathbf{s}$ one can, in principle, compute the time integral in Eq. (24) to determine $c(\mathbf{s},t)$. We "slice" the computation in another way. At a given observation time t we record the positions of all the trajectories and adjust for the last step with an interpolation detailed below.

The random walk simulations are based on numerical solution of the equations of motion (21) and (22), in space and time, for $\mathcal{R}$ different realizations of the joint random processes $\{\mathbf{s}^{(N)},\tau^{(N)}\}_{N=1}^{\infty}$. To suppress large fluctuations of the data, it is necessary to perform the transport simulations for a large number of realizations; we use $\mathcal{R}=10^6$ realizations. The distributions specifying $\mathbf{s}^{(N)}$ and $\xi^{(N)}$, where $\tau^{(N)}=\mathbf{s}^{(N)}\xi^{(N)}$, are discussed in Sec. II and are generated numerically along with their cumulant distributions [e.g., $\Phi(\xi)$ and the integral of $\Phi(\xi)$,$\mathcal{C}(\xi)$ respectively]. The selection from $\Phi(\xi)$, as an example, is chosen using the cumulant distribution: a random number r is generated in the uniform interval [0,1] and set equal to the cumulant $r=\mathcal{C}(\xi)$ and inverted for ξ.

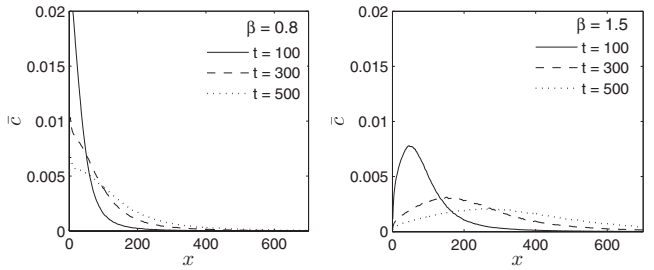

FIG. 3. Vertically integrated plumes $\bar{c}(x,t)$ for the case with $p(s)\sim$TPL with $\alpha=1.8$ and $\Phi(\xi)\sim$ TPL and varying β.

A. Concentration

The determination of the plume at a particular time proceeds as follows: each particle moves as described above through multiple transitions, and at a certain observation time t the position is recorded. In general, the observation time t is within an interval formed by two successive times, i.e., $t^{(N)}\leqslant t<t^{(N+1)}$). A linear interpolation is used such that the particle position at time t is determined according to

$$\mathbf{s}(t)=\mathbf{s}^{(N)}+\frac{t-t^{(N)}}{\tau^{(N)}}\mathbf{s}^{(N)}. \tag{25}$$

B. Breakthrough curves

For breakthrough curves (BTCs) or first passage time distributions, a similar method is employed. Particles are released at [0, 0], and move as described in Eqs. (21) and (22). Once a particle reaches the observation plane at position x_1, the time is recorded. In general, the observation plane lies in the interval formed by successive particle positions $x_1^{(N)}<x_1\leqslant x_1^{(N+1)}$. The actual time $t(x_1)$ when the particle first passes through the observation plane at x_1 is obtained by linear interpolation according to

$$t(x_1)=t^{(N)}+\frac{x_1-x_1^{(N)}}{\mathbf{s}^{(N)}\cos(\omega^{(N)})}\tau^{(N)}. \tag{26}$$

IV. THE DISTRIBUTIONS

In this section we specify a choice of distributions for $\psi(\mathbf{s},t)$ appearing in Eq. (6). For flexibility we use a truncated power-law (TPL) form for $p(s)$ and a modified one for $\Phi(\xi)$. A change in the parameters of these forms can allow a large variation in the character of the distributions, e.g., finite or infinite moments. For the spatial transitions

$$p(s)=C_s\frac{\exp(-s/\lambda_2)}{(c_s+s)^{1+\alpha}}, \tag{27}$$

where C_s is the normalization constant, c_s is a constant, and λ_2 is a cutoff. For $\lambda_2\to\infty$ for finite moments to exist [see the spatial integral in Eq. (12)] $\alpha>d-1+\iota$. In 2D, $\alpha>1$ for $p(s)$ to be normalizable. For $1<\alpha<2$ no moments exist and $p(s)$ is called a Lévy flight distribution. Hence for normal transport (in 2D) for the decoupled case (12), $\alpha>3$. For a slow

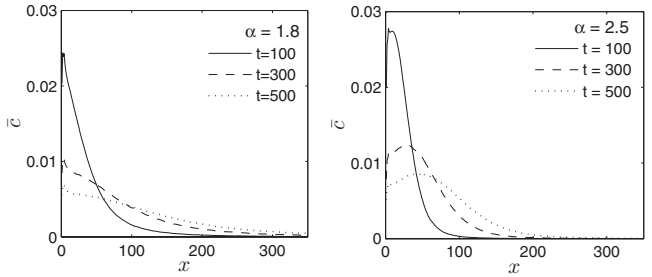

FIG. 4. Vertically integrated plumes $\bar{c}(x,t)$ for the case with $p(s)\sim$TPL and varying α and $\Phi(\xi)\sim$TPL with $\beta=0.8$.

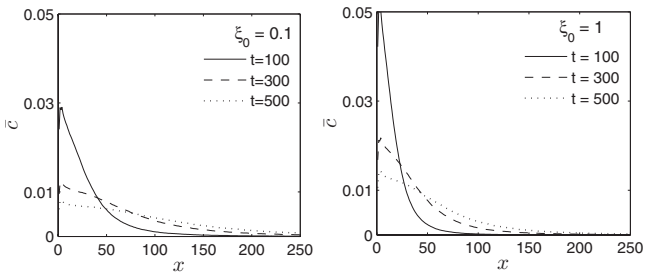

FIG. 5. Vertically integrated plumes $\bar{c}(x,t)$ for $p(\mathbf{s})\sim$TPL ($\alpha=1.8$), and $\Phi(\xi)\sim$TPL ($\beta=0.8$), Υ_e for $\xi_0=0.1,1$.

power law $\alpha<3$ a coupled $\psi(\mathbf{s},t)$ plays a crucial role as we examine in detail.

A. Velocity distributions

1. Constant velocity

We consider the case for which the velocity is the same for all spatial transitions

$$\Phi(\xi) = \delta(\xi - \xi_0). \tag{28}$$

If the form of $p(s)$ is a Lévy flight (power-law tail; see above), this type of delta-coupled CTRW model (28) has been studied in the literature under the name Lévy walk [15,22–25]. Inserting Eq. (28) into Eq. (6) the coupled PDF is

$$\psi(\mathbf{s},t) = p(s)\Omega(\omega)\delta(t - s\xi_0) \tag{29}$$

and the marginal transition time distribution and spatial moments are

$$\psi(t) = tp(t/\xi_0)/\xi_0^2, \quad \mu_i^{(1)}(t) = a_i t^2 p(t/\xi_0)/\xi_0^3,$$
$$\mu_{ij}^{(2)} = b_{ij} t^3 p(t/\xi_0)/\xi_0^4. \tag{30}$$

The moments always exist for this coupled CTRW with constant velocity. Examination of Eq. (29) shows that for any finite value of t the delta function causes $\psi(\mathbf{s},t)$ to vanish when $s \neq t/\xi_0$. Hence, in particular, for large s, i.e., $s > t/\xi_0$, even for a Lévy flight distribution there is an effective cutoff at large s (we return to this issue in the more general case in Sec. IV A 2).

For the corresponding decoupled model, the behavior characterized by

$$\psi_{\mathrm{dc}}(\mathbf{s},t) = F(\mathbf{s})tp(t/\xi_0)/\xi_0^2 \tag{31}$$

is different. For example, the first moment is given by

$$\mu_i^{(1)}(t)_{\mathrm{dc}} = a_i t p(t/\xi_0) \int ds s^2 p(s)/\xi_0^2. \tag{32}$$

The conditions for finite moments of Eq. (32) are discussed for the TPL form of $p(s)$ following Eq. (27) [in Eq. (32), $p(s)$ must decay faster than s^{-3}]. Thus, for a Lévy flight type of transition length distribution, the moments of $\psi_{\mathrm{dc}}(\mathbf{s},t)$ and hence $c(\mathbf{s},t)$ for the decoupled model do not exist (unlike what is claimed in Ref. [26], for example).

The concentration distribution has a clearly defined sharp front in Fig. 2. This reflects the fact that the maximum particle displacement at time t is given by $s^{\max}=t/\xi_0$, which is realized if all the increments $\varsigma^{(n)}$ have $\omega=0$. The minimum (vertically projected) distance $x_1^{\min}=s^{\max}/\sqrt{2}$ [all $\varsigma^{(n)}$ have $\omega=\pi/4$ for Eq. (4)]. In Fig. 2 this spread is seen clearly for the uniform distribution (4). The intermediate paths with varying ω must have $\tau^{(n)}=\varsigma^{(n)}\xi_0$ adding up to t and hence all the $\varsigma^{(n)}$ adding to $s^{\max}$. For the normal distribution (5) the front of the plume is less sharp because $\Omega_n(\omega)$ is peaked about $\omega=0$ but falls off faster around $\omega=0$ than Eq. (4).

Any strongly peaked distribution in velocity such as a Gaussian [basically a broadened version of Eq. (28)] will give rise to plume similar to the ones in Fig. 2, however, with a larger spread due to the width of $\Phi(\xi)$. The transport associated with such plumes is normal.

2. Distributed Velocity

We emphasize a different type of $\Phi(\xi)$, one that gives rise to the power-law in time shown in Fig. 1 and the cutoff region; namely, a truncated power law in ξ. A full range of simulated transport is explored with a $\Phi(\xi)$ encompassing a wide spectrum of velocity

$$\Phi(\xi) = C_\xi \Upsilon(\xi) \frac{\exp(-\xi/\lambda_1)}{(c_\xi + \xi)^{1+\beta}}, \tag{33}$$

where we use for $\Upsilon(\xi)$ two different types of dependence for the low ξ behavior,

$$\Upsilon_e(\xi) = \exp(-\xi_0/\xi), \quad \Upsilon_\eta(\xi) = \frac{(\xi/\xi_1)^\eta}{1 + (\xi/\xi_1)^\eta}, \tag{34}$$

where C_ξ is the appropriate normalization constant, c_ξ is a constant and λ_1 is a cutoff. The forms for $\Phi(\xi)$ in Eqs. (33) and (34) are chosen to provide flexibility in the character of the velocity spectrum. The high ξ dependence has the form of a truncated power law (TPL), which gives rise to a power-law time dependence associated with non-Fickian transport [18], i.e., it replicates the form, derived analytically, in Fig. 1. The power-law time dependence has been established in a number of studies [5] and discussed in Sec. I. In contrast a power-law tail with velocity for the velocity spectrum would not exhibit this behavior. In addition to being in disagreement with numerical studies of the latter, e.g., Ref. [9], it would suppress the role of the statistically rare low velocities that limit the transport—a key feature giving rise to non-Fickian transport [5]. The cutoff at λ_1 in the TPL form in Eq. (33) is a control of the width of this time power-law tail. The

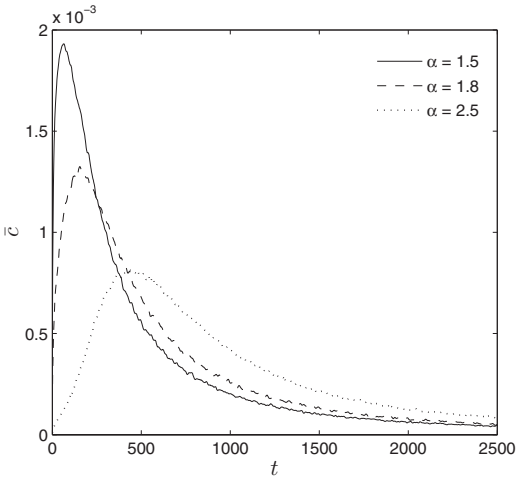

FIG. 6. First passage time distribution (at $x_0=100$) resulting from a variable α for the $p(\mathbf{s})$, and $\Phi(\xi)\sim$TPL with $\beta=0.8$ (Fig. 4).

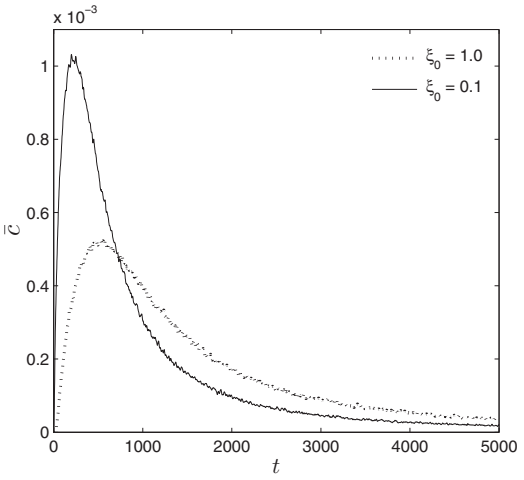

FIG. 7. First passage time distribution (at $x_0=100$) for the $p(\mathbf{s})\sim$TPL ($\alpha=1.8$), and $\Phi(\xi)\sim$TPL ($\beta=0.8$) Υ_e, for $\xi_0=0.1,1$ (Fig. 5).

$\Upsilon(\xi)\underset{\xi\to 0}{\to}1$ for $\xi/\xi_0>1$ or $\xi/\xi_1>1$ and most importantly $\Upsilon(\xi)\underset{\xi\to 0}{\to}0$. The importance of the latter behavior can be seen by examining Eqs. (7) and (8) for a $p(s)$ with a power-law tail [the integrals with $p(s)$ (27) without the effective cutoff, $\lambda_2\to\infty$, for large s, can diverge]. The forms $\Upsilon(\xi)$ in Eq. (34) were chosen to allow an ability (with one parameter ξ_0 or η) to vary the approach to the physical limit $\Upsilon(\xi)\underset{\xi\to 0}{\to}0$.

For the Lévy flight case of $p(s)$, the moments in Eqs. (7) and (8) are all finite if $\Phi(\xi)$ [or as we insert $\Phi(t/s)/s$] approaches zero sufficiently fast. This certainly is the case for $\Upsilon_e(\xi)$ and for $\Upsilon_\eta(\xi)$ for $\eta>d-2+\iota-\alpha$ in Eq. (34). Hence, the small ξ behavior of $\Phi(\xi)$ controls the finite values of the spatial moments for the coupled case in Eq. (7) for a Lévy flight. It is the high ξ behavior of $\Phi(\xi)$ that controls the non-Fickian behavior associated with the statistically rare long time transitions. The small ξ dependence of $\Phi(\xi)$ additionally can enhance the probability of long displacements by providing enough high velocities to include these transitions in any given time interval t. For Lévy behavior of $p(s)$ (even when $\lambda_2<\infty$) the range of transport phenomena depends on the entire velocity spectrum, not only the high ξ tails as has been emphasized for many cases in the literature [5]. For these cases, however, the $p(s)$ has a compact or finite range and the high ξ tail dominates the transport, so much so that a decoupled approximation is valid (as we will examine) and a TPL form of $\psi(t)$ is acceptable [$\psi(t)\underset{t\to 0}{\to}$ const, which implies an infinite velocity but with finite displacements]. The finite spatial moments for the coupled $\psi(\mathbf{s},t)$ for Lévy spatial power tails indicate that we can use these types of joint distributions in Eqs. (24)–(26) of Ref. [5] that define a partial differential equation form of CTRW. Here we now investigate plume shapes and BTCs for $\psi(\mathbf{s},t)$ in Eq. (6)—for $\Phi(\xi)$ and $p(s)$ in Eqs. (33), (34), and (27) as a function of the parameter space formed by $\xi_0,\xi_1,\eta,\lambda_1,\lambda_2,\beta,\alpha$—in order to study the competition between long displacement and long time transitions and the range of validity of the decoupled approximation (11).

V. RESULTS AND DISCUSSION

A. Forward and backward tails

In Figs. 3–10 we explore the transport phenomena generated by the coupled $\psi(\mathbf{s},t)$ as defined by Eqs. (33), (34), and (27) through the coupling $t=s\xi$. Unless stated otherwise the value of $\lambda_{1,2}=10^5$ and we use Υ_e in Eq. (34). In Fig. 3, $\bar{c}(x,t)$, the vertically integrated plume (subsequently referred to as plume) evolution at three different times is compared with $\alpha=1.8$ and $\beta=0.8,1.5$. The plumes behave in the expected way [5] with this variation in the time power law [18], however, with the added forward displacement tails due to the Lévy-like contribution of $p(s)$ with $\alpha=1.8$. This contribution can be more clearly discerned in Fig. 4 as we decrease the contribution of the Lévy-like $p(s)$ by varying α from 1.8 to 2.5. With fixed $\beta=0.8$ the long time tail transitions should dominate the plume shape but the change in α alone changes the character of the plume shape significantly.

B. The entire velocity spectrum plays a role

In Fig. 5 we vary the effect of $\Upsilon_e(\xi)$, i.e., ξ_0. The increase in the high velocity component ($\xi_0=0.1$) leads to a larger

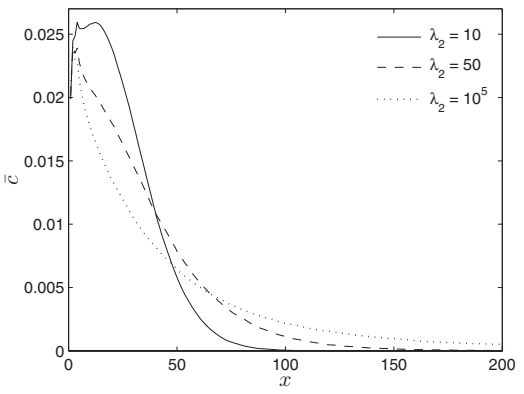

FIG. 8. Vertically integrated plumes, $\bar{c}(x,t)$, for the case where we vary the spatial tail (λ_2) of $p(s)\sim$TPL with $\alpha=1.5$ and $\Phi(\xi)\sim$TPL with $\beta=0.8$.

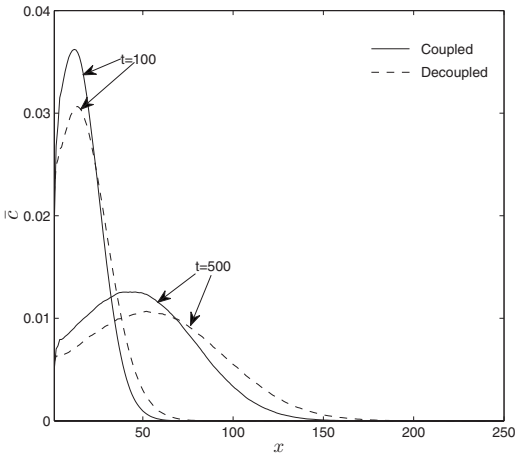

FIG. 9. Coupled vs decoupled time evolution. For both cases, $p(\mathbf{s}) \sim$ TPL (α=2.5), and for the coupled $\Phi(\xi) \sim$ TPL (β=0.8), for the uncoupled $\psi(t) \sim$ TPL (β=0.8). The λ cutoff for both $p(\mathbf{s})$ is 5.

profile displacement. The high velocity portion of Eq. (33), controlled by Eq. (34), enables large displacements from Eq. (27) to contribute within the time window. It is evident now that with a coupled $\psi(\mathbf{s},t)$ and a Lévy-like $p(s)$ the entire velocity spectrum plays a role in shaping the plume propagation. The BTCs (or first passage time distributions) are a sensitive measure of the degree of forward tailing. In Fig. 6 the variation of the spatial power-law with α changing from 1.5 to 2.5 (Fig. 4) produces a major redistribution of the particle arrival time at a control plane (x_0=100). The softer tail (α=1.5) causes the BTC to peak at a significantly earlier time than the α=2.5 resultant shape. In Fig. 7 the effect of changing the high velocity component of Eq. (33) in Fig. 5 can be seen clearly. The degree of forward tailing causes a large shift in the BTC peak position. Hence, a feature of $\Phi(t/s)$ not associated with the long time power-law tail can have a strong effect on the character of the $\bar{c}(x,t)$ propagation. The results with Υ_η in Eq. (34) with η=2 are nearly identical to the ξ_0=0.1.

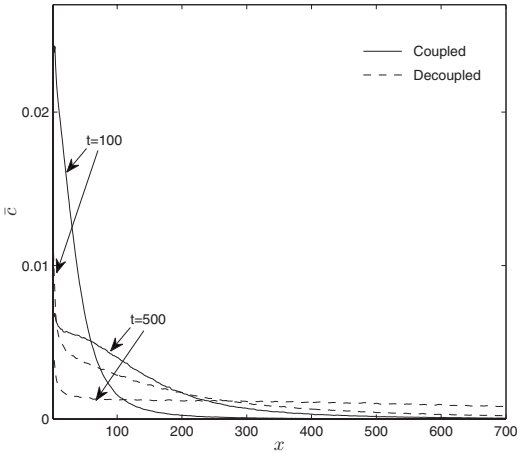

FIG. 10. Coupled vs decoupled time evolution. For both cases, $p(\mathbf{s}) \sim$ TPL (α=1.8), and for the coupled $\Phi(\xi) \sim$ TPL (β=0.8), for the uncoupled $\psi(t) \sim$ TPL (β=0.8). The λ cutoff for both $p(\mathbf{s})$ is 10^5.

TABLE I. The exponents of the time dependence of the spatial moments of the vertically integrated plume $\bar{c}(x,t)$, $m_1(t) \propto t^{\gamma_1}$ and the standard deviation $\sigma(t) \propto t^{\gamma_2}$ for various α and β.

Parameters	γ_1	γ_2
α=1.8, β=0.8	0.70	0.50
α=2.5, β=0.8	0.68	0.57
α=1.8, β=1.5	0.77	0.47
α=2.5, β=1.5	0.87	0.64

C. Spatial cutoff: Coupled versus decoupled

In Fig. 8 we exhibit the effect of varying the extent of the spatial tail by changing the cutoff λ_2 from 10 to 10^5 at a fixed value of α(=1.5). The character of $\bar{c}(x,t)$ is dramatically different with a "compact" $p(s)$ vs a long Lévy tail $p(s)$. The significance of this difference is shown in Figs. 9 and 10. In Fig. 9 a comparison is made between the coupled and decoupled case for the same parameters. For a compact $p(s)$ (λ_2=5) the coupled and decoupled case are similar. However in Fig. 10 a comparison is made between the coupled and decoupled case for the same parameters for a Lévy-like $p(s)$ ($\lambda_2=10^5$). The plume for the coupled case is the same shown on the left side of Fig. 3 and was discussed above. The decoupled case shown in Fig. 10 differs considerably from the one in the literature (for β=0.8) [18]. The latter has a decoupled $p(s)$ of a Gaussian form while in Fig. 10 the corresponding $p(s)$ is a power law (α=1.8) with a large cutoff ($\lambda_2=10^5$), which enhances the plume propagation with unconstrained large displacements. For the coupled case these displacements are constrained by the link $s=t/\xi$. The main point is to contrast the two cases and they are definitely dissimilar. This is a basic result: the decoupled $\psi(\mathbf{s},t)$ approximation used extensively in the literature holds well if the spatial distribution has a limited or compact range. For those applications that involve a large extent of a soft power-law in the spatial distribution, $\psi(\mathbf{s},t)$ must be used in the coupled form. The compactness of $p(s)$ can be quantified by the agreement of the approximation

$$\mu^{(\iota)}(t) \approx \int_0^\infty ds s^{d-1} s^\iota p(s) \Phi(t/\bar{s})/\bar{s} + \cdots , \tag{35}$$

to Eq. (8), where the dots denote subleading contribution of the order of the variance of $p(s)$ and $\bar{s}$ is the first moment of $p(s)$ [the spatial integral in Eq. (12) with ι=1]. Expression (35) decouples all of the moments of $\psi(s,t)$. The distribution that is actually characterized by the moments (35) is precisely the decoupled distribution

$$\psi_{\mathrm{dc}}(\mathbf{s},t) = F(\mathbf{s}) \Phi(t/\bar{s})/\bar{s}. \tag{36}$$

D. Moments

In Table I we show the time dependence of the first moment and standard deviation of $\bar{c}(x,t)$ in the form

$$m_1(t) \propto t^{\gamma_1}, \quad \sigma(t) \propto t^{\gamma_2}, \tag{37}$$

where $\sigma(t)$ is defined in Eq. (20). For the values of α and β, corresponding to Figs. 3 and 4 the exponents show that the transport is anomalous or non-Fickian. The exponents are determined numerically from these plumes. The relations among the exponents are not the same as those derived from plumes generated in the decoupled case with $\psi(t) \propto t^{-1-\beta}$ [18]. In that case the first moment $m_1(t) \propto t^{\beta}$ and the standard deviation $\sigma \propto t^{\beta}$ for $0<\beta<1$ and $m_1(t) \propto t$, $\sigma \propto t^{(3-\beta)/2}$ for $1<\beta<2$. We emphasize that we are comparing the relative values of the exponents $\gamma_{1,2}$ for a coupled case (Table I), with power laws for both space and time, with the usual decoupled case with a compact $p(s)$ and a power-law in time [18]. For $\beta=0.8$ in Table I there is a close proximity to the latter result with $\gamma_1 \approx \beta$, however, this is not the case for the standard deviation with $\gamma_2 < \beta$. The slower growth in time of the standard deviation is a subtle effect and could be due to the competition between long time tail behavior and large displacements constrained by $s=t/\xi$. The large time tail tends to both promote solute localization (near the origin) and a freely moving forward tail. The $p(s)$ power-law changes the mix with the addition of constrained large displacements, i.e., less localization near the origin. For $\alpha=2.5$ with the same $\beta(=0.8)$ the main change is in the growth of the time dependence of $\sigma(t)$ (i.e., less large displacements). For $\beta=1.5$ the effects of the time tail are less dominant (for $\alpha=1.8$, $\gamma_1<1$) and the Lévy contribution is more discernible, i.e., there is an increase in the non-Fickian behavior. There is a larger change in $\gamma_{1,2}$ with the change in α to 2.5: $\gamma_1 \lessapprox 1$ and the standard deviation ($\gamma_2=0.64$) approaches the decoupled value of 0.75. The overall effect of the coupling of a power-law in both space and time is to enlarge the range of anomalous transport behavior.

E. Potential applications

This enlarged range of behavior opens up application possibilities. We have alluded to two potential applications in the abstract. There are others for a coupled CTRW with power laws in space and time, but we concentrate on those generated by a velocity distribution, i.e., the particle transitions are "carried" by a moving fluid. In Ref. [27] we analyzed a RFN by limiting the particle transitions to fracture fragments, i.e., the displacements were between fracture junctions. We conjectured about possible correlations due to the higher velocities in a portion of the fragments. At these velocities the sequential particle could be correlated (it could involve a change from a diffusive condition at the junction to a streamline one). The coupled $\psi(\mathbf{s},t)$ we have been discussing in Sec. IV A 2 can provide a statistical correlation of this type whereby the range of higher velocities can provide larger displacements than the nominal ones. This would require relating the statistics of these events into the characterization of $\psi(\mathbf{s},t)$.

In Ref. [19] a study was made of correlation lengths and times of the Lagrangian flow velocity in log normal permeability model fields; Refs. [28,29] also consider highly heterogeneous media. The aim is to relate these correlations, coupled by the relation $s\xi=t$, to transport behavior. A natural place to relate the statistical basis of correlation lengths as a function of velocity and link to the correlation time is the coupled $\psi(\mathbf{s},t)$.

F. Concluding remarks

The CTRW with a coupled $\psi(\mathbf{s},t)$ with both a power-law in time as well as in space, with finite spatial moments, has enriched the scope of transport behavior. Subtle features of the entire velocity spectrum, e.g., the small ξ component, have demonstrable effects on the first passage time (BTCs). The Lévy spatial power law adds to the dispersion even in presence of a soft power law in time. The decoupled approximation is valid with a decrease in this added dispersion, i.e., a more compact $p(s)$. The enhanced transport features of this coupled $\psi(\mathbf{s},t)$ give rise to a broader scope of applications, e.g., to correlated migrations in RFN and in heterogeneous permeability fields [19] discussed in the previous section.

ACKNOWLEDGMENTS

M.D. gratefully acknowledges the financial support of the program "Ramon y Cajal" of the Spanish Ministry of Education and Science (MEC), ENRESA (Empresa Nacional de Residuos Radioactivos), the European Union IP FUNMIG (Contract No. 516514), and the MEC project MODEST (Project No. CGL-2005-05171). B.B. thanks the Sussman Family Center of Environmental Research for financial support.

[1] J. P. Bouchaud and A. Georges, Phys. Rep. **195**, 127 (1990).
[2] P. Lallemand-Barres and P. Peaudecerf, Bull. Bur. Rech. Geol. Min. Fr. (Sect. 3) **4**, 277 (1978).
[3] J. Eggleston and S. Rojstaczer, Water Resour. Res. **34**, 2155 (1998).
[4] L. W. Gelhar, *Stochastic Subsurface Hydrology* (Prentice-Hall, Englewood Cliffs, 1993).
[5] B. Berkowitz, A. Cortis, M. Dentz, and H. Scher, Rev. Geophys. **44**, RG2003 (2006).
[6] B. Berkowitz and H. Scher, Phys. Rev. E **57**, 5858 (1998).
[7] A. Cortis, Y. Chen, H. Scher, and B. Berkowitz, Phys. Rev. E **70**, 041108 (2004).
[8] G. Di Donato, E.-O. Obi, and M. J. Blunt, Geophys. Res. Lett. **30**, 1608 (2003).
[9] B. Bijeljic and M. J. Blunt, Water Resour. Res. **42**, W01202 (2006).
[10] M. V. Kohlbecker, S. W. Wheatcraft, and M. M. Meerschaert, Water Resour. Res. **42**, W04411 (2006).
[11] X. Zhang and M. Lv, Water Resour. Res. **43**, W07437 (2007).

[12] A. Fiori, I. Janković, G. Dagan, and V. Cvetković, Water Resour. Res. **43**, W07445 (2007).
[13] P. Lévy, *Théorie de l'Addition des Variables Alé atoires* (Gauthier Villars, Paris, 1937).
[14] B. B. Mandelbrot, Int. Econom. Rev. **1**, 79 (1960).
[15] J. Klafter, A. Blumen, and M. F. Shlesinger, Phys. Rev. A **35**, 3081 (1987).
[16] P. Levitz, Europhys. Lett. **139**, 593 (1997).
[17] R. Metzler and J. Klafter, Phys. Rep. **339**, 1 (2000).
[18] M. Dentz, A. Cortis, H. Scher, and B. Berkowitz, Adv. Water Resour. **27**, 155 (2004).
[19] T. Le Borgne, J. R. De Dreuzy, P. Davy, and O. Bour, Water Resour. Res. **43**, W02419 (2007).
[20] H. Scher and M. Lax, Phys. Rev. B **7**, 4491 (1973).
[21] H. Risken, *The Fokker-Planck Equation* (Springer, Berlin, 1996).
[22] M. F. Shlesinger, B. J. West, and J. Klafter, Phys. Rev. Lett. **58**, 1100 (1987).
[23] J. Klafter, A. Blumen, G. Zumofen, and M. F. Shlesinger, Physica A **168**, 637 (1990).
[24] M. F. Shlesinger, Nature (London) **411**, 641 (2001).
[25] V. Y. Zaburdaev, J. Stat. Phys. **123**, 871 (2006).
[26] H. C. Fogedby, Phys. Rev. E **50**, 1657 (1994).
[27] B. Berkowitz and H. Scher, Phys. Rev. Lett. **79**, 4038 (1997).
[28] T. Le Borgne, M. Dentz, and J. Carrera, Phys. Rev. E (to be published).
[29] T. Le Borgne, M. Dentz, and J. Carrera, Phys. Rev. E (to be published).